

Three ways in, one way out: Water dynamics in the trans-membrane domains of the inner membrane translocase AcrB

Nadine Fischer and Christian Kandt*

Computational Structural Biology, Department of Life Science Informatics B-IT, Life & Medical Sciences (LIMES) Center, University of Bonn, Bonn 53113, Germany

ABSTRACT

Powered by proton-motive force, the inner membrane translocase AcrB is the engine of the AcrAB-TolC efflux pump in *Escherichia coli*. As proton conduction in proteins occurs along hydrogen-bonded networks of polar residues and water molecules, knowledge of the protein-internal water distribution and water-interacting residues allows drawing conclusions to possible pathways of proton conduction. Here, we report a series of 6×50 ns independent molecular dynamics simulations of asymmetric AcrB embedded in a phospholipid/water environment. Simulating each monomer in its proposed protonation state, we calculated for each transmembrane domain the average water distribution, identified residues interacting with these waters and quantified each residue's frequency of water hydrogen bond contact. Combining this information we find three possible routes of proton transfer connecting a continuously hydrated region of known key residues in the TMD interior to bulk water by one cytoplasmic and up to three periplasm water channels in monomer B and A. We find that water access of the transmembrane domains is regulated by four groups of residues in a combination of side chain reorientations and shifts of trans-membrane helices. Our findings support a proton release event via Arg971 during the C intermediate or in the transition to A, and proton uptake occurring in the A or B state or during a so far unknown intermediate in between B and C where cytoplasmic water access is still possible. Our simulations suggest experimentally testable hypotheses, which have not been investigated so far.

Proteins 2011; 00:000–000.
© 2011 Wiley-Liss, Inc.

Key words: membrane protein; multi-drug efflux; proton transfer; molecular dynamics simulation; transport; antibiotics resistance.

INTRODUCTION

Since the first observations over a century ago,¹ microbial resistance to antibiotics has developed into one of the major challenges in biomedical research today. Major strategies by which bacteria achieve antibiotics resistance include inactivation of the drug, modification of the drug target and prevention of drug access to its target molecule.² A prominent example of the latter mode of action is drug expulsion by an over-production of multi-drug (MDR) efflux pumps which to date have been identified in five ubiquitous protein superfamilies and one small eukaryotic-specific family.³ Whereas members of the ATP binding cassette (ABC) superfamily resort to ATP hydrolysis to power drug transport, MDR efflux pumps of the major facilitator (MFS), multi antimicrobial extrusion (MATE), drug/metabolite transporter (DMT), and resistance/nodulation/division (RND) superfamilies function by drug:cation antiport mechanisms.³

Since its discovery 17 years ago,⁴ the inner membrane translocase acriflavine resistance protein B (AcrB) has become the best studied member of the RND superfamily.⁵ Functioning as the engine of the tripartite MDR efflux pump AcrAB-TolC in *Escherichia coli*,^{4,6,7} AcrB recognizes and binds a broad palette of substrates^{8–10} using proton-motive force to drive drug expulsion in the assembled pump.^{9,11,12} Whereas the first crystal structure showed identical monomer conformations in the AcrB trimer,¹³ following X-ray studies revealed a structural asymmetry among the monomers, each trapped in a different conformation.^{14–16} Interpreted as reaction cycle intermediates “loose/access” (monomer A), “tight/binding” (monomer B), and “open/extrusion” (monomer C) in a peristaltic pump mechanism,^{14–16} the different monomer conformations have been found interdependent and complementarily adaptive^{17–19} representing an essential precondition for AcrB pump activity since inactivation of a single monomer leads to a complete activity loss of the entire trimer.²⁰

Similar to ABC transporters^{21,22} substrate transport and energy conversion in AcrB occur in spatially separated parts of the protein.

Additional Supporting Information may be found in the online version of this article.

*Correspondence to: Christian Kandt, Computational Structural Biology, Department of Life Science Informatics B-IT, Life & Medical Sciences (LIMES) Center, University of Bonn, Dahlmannstr 2, Bonn 53113, Germany. E-mail: kandt@bit.uni-bonn.de

Received 25 January 2011; Revised 3 June 2011; Accepted 10 July 2011

Published online 15 July 2011 in Wiley Online Library (wileyonlinelibrary.com).

DOI: 10.1002/prot.23122

Proton transfer from periplasm to cytoplasm through the trans-membrane domain (TMD) yields the energy driving the transport-relevant conformational changes in the periplasmic porter and docking domains.^{18,19,23} As proton conduction in proteins occurs along hydrogen-bonded networks of polar residues and water molecules²⁴ in a Grotthuss-like mechanism,^{25–28} knowledge of the protein-internal water distribution and interacting residues allows drawing conclusions to possible pathways of proton conduction.^{29–35} Compared to other proton pumps such as bacteriorhodopsin,^{36,37} our current level of understanding of the AcrB proton conduction pathway is still at the beginning. To date, the distribution of AcrB-internal water is unknown, and five TMD residues have been identified whose mutation to alanine leads to a loss of function of >90%.^{13,38–41} For these residues intermediate-specific protonation states have been proposed,¹⁷ based on their side chain conformations in the asymmetric AcrB crystal structures.^{14–16}

Whereas previous computational studies have focused on assessing overall AcrB flexibility via elastic network normal mode analysis⁴² and investigating conformational cycling and drug transport using all-atom targeted molecular dynamics of the membrane-embedded trimer⁴³ and coarse-grained multiple-basin simulations of the isolated AcrB porter domains,⁴⁴ here we report unbiased all-atom AcrB molecular dynamics simulations to investigate protein-internal water dynamics. Addressing the questions of TMD hydration, possible proton conduction pathways and new key residues candidates, we performed a series of 6×50 ns independent molecular dynamics simulations of asymmetric, substrate-free AcrB¹⁵ in a phospholipid/water environment. Simulating the currently proposed protonation scenario,¹⁷ we calculated for each monomer water residence probabilities in form of mean water densities,^{32,33} identified all residues in the AcrB hydrogen-bonded network and computed their average frequency of hydrogen bond contact to TMD-internal water. Although the explicit simulation of proton transfer requires at least partially a quantum mechanical treatment,^{27,45–50} earlier studies^{30,32,33} demonstrated, that classical MD can produce insightful results following a similar approach as employed here. We find that TMD water distribution is monomer-specific. Whereas periplasmic and cytoplasmic bulk water are transiently connected via a continuously hydrated and key residue-encompassing core region in monomer A and throughout the entire simulation time in monomer B, there is no bulk water access in monomer C. Further, with the exception of monomer C, TMD hydration is also asymmetric within each monomer with up to three water channels leading to the core region from periplasmic side but only a single water channels connecting to cytoplasmic bulk water. Combining the information of average water distribution and residue water H-bond frequency together with conformational changes between the

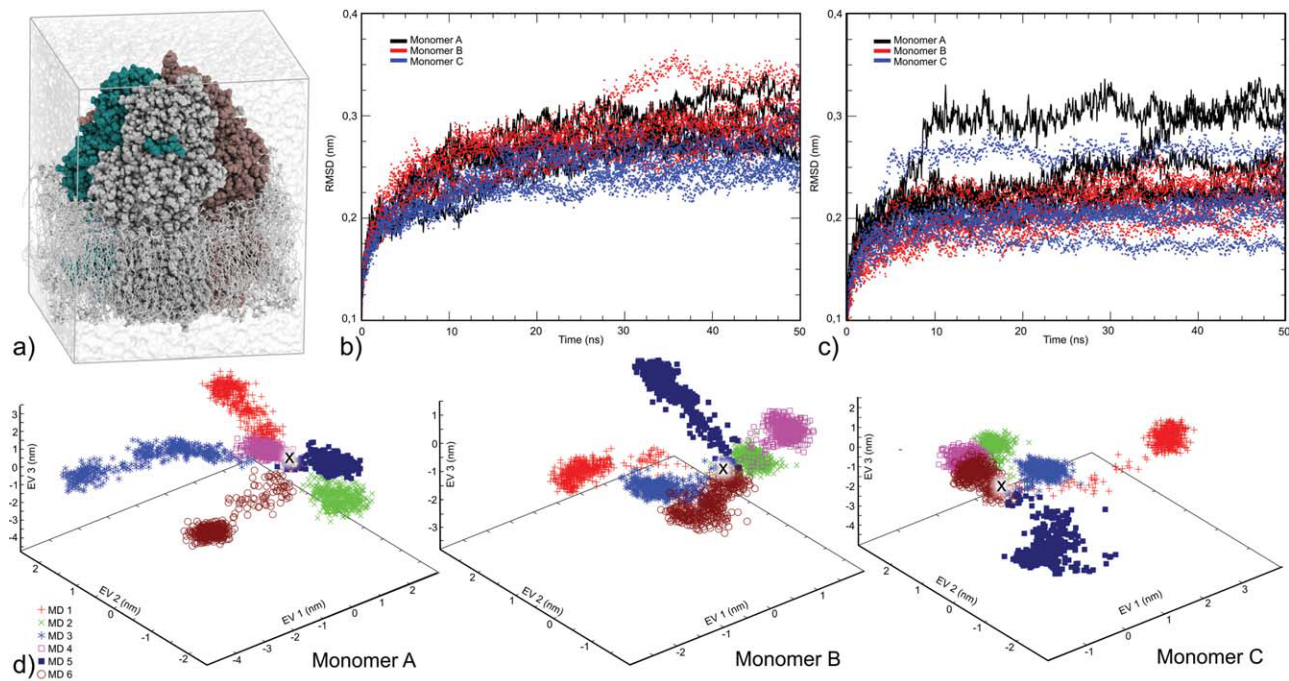
monomers, we identify three groups of new key residue candidates: (a) framework residues lining the mean water densities and providing the scaffold for TMD water organization, (b) four groups of gating residues regulating TMD bulk water access in a combination of side chain re-orientations and shifts of trans-membrane helices, and (c) three negatively charged TMD surface residues, which might act like proton antennas attracting water molecules to the mouths of two periplasmic water channels, located at or below the level of lipid head groups. With bulk water access present in the A and B states but not in C, our data suggest that proton uptake occurs either in a so far unknown intermediate between B and C or during the A or B state with the third excess proton transiently stored in a protonated water cluster until the C intermediate is reached. With direct bulk water contact in C, our findings support Arg971-H as likely proton release group candidate, deprotonating either in the C intermediate or during the transition to A.

MATERIALS AND METHODS

Simulation details

Molecular dynamics simulations were performed using the GROMACS 4.0.3 package^{51,52} and GROMOS96 53a6 force field.⁵³ The asymmetric 2.9 Å 2GIF AcrB crystal structure¹⁵ was used as starting structure. The protein was inserted in a pre-equilibrated 14 × 14 nm palmitoyloleoyl-phosphatidylethanolamine (POPE) bilayer using INFLATEGRO as detailed in Reference 54 except for applying a scaling factor of 2 in the expansion and 0.98 in the compression phase. The POPE bilayer was built from an initial 9.6 × 9.5 nm POPE patch⁵⁵ that was enlarged and equilibrated for 20 ns. Simulation settings were the same as for the AcrB runs given below. To solvate AcrB's central lipid-filled cavity, 23 POPE molecules were placed manually by selecting from a superimposed pre-equilibrated POPE bilayer lipid molecules whose head groups did not clash with the surrounding protein. Where necessary, lipid tail dihedrals were adjusted to remove steric clashes. 14 lipids were found in the upper and 9 in the lower leaflet. The final simulation system comprises 3108 protein residues, 457 POPE lipids, 49521 simple point charge water molecules,⁵⁶ 273 sodium ions and 230 chloride ions yielding a 150 mM NaCl solution and total system charge of zero [Fig. 1(a)]. Except for Asp407, Asp408, Lys940, and Arg971, which were protonated according to,¹⁷ standard protonation states were assumed for titratable residues.

Similar to^{57–59} a series of 6×50 ns independent and unrestrained MD simulations was performed; each initiated using a different temperature seed number to generate the random distribution of starting velocities. The production runs were preceded by a 30 ns membrane equilibration where all non-hydrogen protein atoms were

**Figure 1**

The full 2GIF AcrB trimer was simulated in POPE/water environment at a 150 mM NaCl concentration (a). To assess the degree of conformational sampling in our simulations we calculated C α root mean square deviations of the entire AcrB monomers (b) and the trans-membrane domains (c) and performed for each monomer a principal component analysis of the C α atoms in the trans-membrane domain (d).

position-restrained applying a force constant of 1000 kJ/mol/nm². In the simulations, all bond lengths were constrained by LINCS so that an integration time step of 2 fs could be chosen.⁶⁰ Systems were simulated at a temperature of 310 K, maintained separately for protein, lipids and water + ions by a Berendsen thermostat⁶¹ with a time constant of $\tau_T = 0.1$ ps. A Berendsen barostat⁶¹ was applied using semi-isotropic pressure coupling with time constants of 4 ps and reference pressures of 1 bar for the contributions in Z and XY directions. Electrostatic interactions were calculated using particle mesh Ewald summation^{62,63} and twin range cut-offs of 1.0 and 1.4 nm were applied for computing the van der Waals interactions.

Analysis

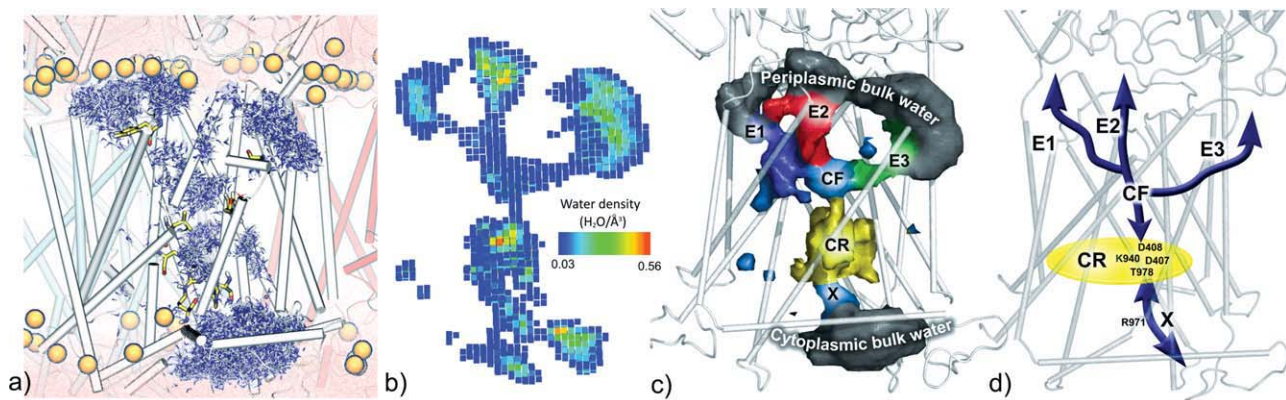
Conformational sampling

The amount of conformational sampling in the simulations was assessed on the level of backbone and side chain dynamics. Next to standard C α root-mean square displacements RMSD [Fig. 1(b,c)], each monomer's path through conformational space was determined and mapped down to three dimensions of the first three Eigenvectors in a principal component analysis of the TMD C α atoms [Fig. 1(d)]. To this end all six simulations were concatenated and analyzed separately for each monomer. As side chain conforma-

tion is to a large degree determined by the χ_1 and χ_2 dihedrals around the C α -C β and C β -C γ bond, each monomer's χ_1/χ_2 distribution was calculated for all six simulations. To focus on residues interacting with TMD water, the analysis was restricted to all side chains that in the monomer TMD average structure are located within a 2.0 Å distance cut-off of the monomer B water densities run-averaged over the first third of simulation time (see below).

Water dynamics in the trans-membrane domains

Analogous to^{32,33,58,64} the TMD-internal water distribution was computed as mass-weighted water densities using the VolMap tool in VMD 1.8.7.⁶⁵ For each monomer the water densities were recorded at 1 Å³ resolution after C α -fitting the trajectories to the average TMD monomer conformation. Average structures were determined using an iterative scheme of calculating the average conformation and re-aligning the trajectory to that average structure to compute a new average structure. This procedure was repeated until the average structure stopped changing. Four types of water densities were calculated: (1) To determine the overall TMD water distribution, run-averaged water densities were computed over all six simulations for the entire 50 ns simulation time. (2) To reflect the TMD hydration during the simulation time selected

**Figure 2**

TMD internal water molecules (blue sticks) were detected based on a 8 Å cut-off around a set of 11 residues (yellow sticks) distributed along the TMD Z-axis (a). For each monomer the average water distribution was computed as voxel-based, mass-weighted mean water densities (b). Voxels exceeding a water density of 0.03 H₂O/Å³ were visualized by enveloping Connolly surfaces using a probe sphere radius of 1.4 Å (c). TMD water is organized in a key residue encompassing core region (CR) connected to bulk water by one cytoplasmic (X) and up to three periplasmic water channels (E1-E3) (c and d). In a conflux region (CF) the E1-3 channels merge into a single channel before reaching the core region.

for the hydrogen bond analysis (see below), run-averaged water densities were calculated over the last 25 ns simulation time. (3) To test whether each monomer's TMD hydration pattern is constant or dynamic, run-averaged water densities were calculated over thirds (0–17 ns, 17–35 ns, 35–50 ns) of the simulation time. (4) To monitor the opening state of each of the four water channels in each monomer, water densities were computed over time windows of 10 × 5 ns for each of the six simulations. In this analysis a channel was considered open when it contained water for at least half of the 5 ns observation time which was found corresponding to a water density of 0.2 H₂O/Å³. For the run-averaged water densities the resulting OpenDX voxels were averaged into a single data set after conversion into PDB format via dxTuber⁶⁶ encoding each voxel's water density as formal B-factor.

To reduce computational cost, only a subset of the 49,521 waters in the system was considered in the Vol-Map analysis representing all water molecules at least transiently located inside the TMDs. The water subset was defined based on an 8 Å distance cut-off around a set of eleven residues distributed along the TMD Z-axis, that were found to encompass all TMD-internal waters in each monomer in all trajectories [Fig. 2(a)]. The residues included in this set are Glu414, Arg971, Asp407, Lys940, Leu937, Phe982, Phe927, Phe988, Phe974, Val411, and Thr933. For visualization and analysis of the voxel-based water distributions, we focus on regions of high residence probability [Fig. 2(b)] characterized by voxels displaying a mean water density of at least 0.03 H₂O/Å³, which is the value for bulk water under standard conditions. For the enveloping Connolly surfaces [Fig. 2(c)] a probe radius of 1.4 Å was used.

To analyze the direction of water flow through the TMD, we monitored in all simulations the Z-coordinate of all waters at least transiently TMD-internal, counting the water molecules entering or leaving the TMD on periplasmic or cytoplasmic side. TMD-internal waters in this analysis were identified combining two water subsets comprising all waters found at least once within a 5 Å distance of (a) the center of mass of Asp407, Asp408, and Lys940 or (b) the center of mass the conflux region residues (Table I).

Frequency of hydrogen bond contact

Similar to^{32,33} the GROMACS tool g_hbond was used to identify residues forming hydrogen bonds to TMD-internal water molecules. Determining H-bonds based

Table I

Residues Lining the Six Regions of the TMD Water Distributions

Region	Residue
E1 channel	Phe556 Ser561 Tyr877 Val909 Asn923 Phe927 Gln928 Leu931
E2 channel	Val912 Leu916 Leu921 Phe927 Gly930 Leu931 Ala1002 Thr1005 Gly1006
E3 channel	Thr343 Glu346 Ala347 Leu350 Gly985 Val986 Ser988 Leu989
Conflux region	Val399 Leu400 Ile402 Gly403 Leu404 Thr933 Leu937 Phe982 Leu989 Thr1005 Val1007 Met1011
Core region	Ala371 Val375 Gly403 Leu404 Leu405 Val406 Asp407 Asp408 Leu443 Ile446 Met478 Ser481 Val484 Thr489 Leu881 Val884 Val901 Met902 Val905 Gly908 Val909 Thr934 Ile935 Leu937 Ser938 Ala939 Lys940 Asn941 Arg971 Thr978 Phe982 Met1011 Thr1015
X channel	Val411 Leu442 Leu944 Arg971 Pro974 Phe948 Arg418 Ile975

on a donor-acceptor distance (max 3.5 Å) and acceptor-donor-hydrogen angle cut-off (max. 30°), g_hbond produces time-resolved H-bond occurrence maps for each water–residue pair that comes into H-bond contact at least once throughout the simulations. For computational efficiency, not all possible interaction partners among the 3108 protein residues and 49521 water molecules were considered. Instead we focus on a selection of groups of interest in a two-step g_hbond analysis. As Asp407, Asp408, Lys940, Arg971, and Thr978 have already been identified as relevant for AcrB proton transfer,^{38–41} we regard these as “initial” set of residues we use to begin our analysis. This set is complemented by an additional group of residues (Supporting Information Table S1) we found lining the TMD-internal water distributions in our simulations. By a first H-bond analysis, where all waters but only the “initial” set residues were considered, we determined a subset of “essential” water molecules that were at least transiently interacting with the key residues. In a second H-bond analysis we monitored the behavior of these waters against all protein residues in order to identify further TMD residues forming H-bonds with the water subset. Analogous to³³ this eventually yields a complete list of AcrB residues that are, at least temporarily, in contact with essential water molecules. For each such residue in the trans-membrane domain of each monomer the average frequency of H-bond contacts was computed as percentage of the last 25 ns simulation time and averaged over all six trajectories.

All molecular illustrations were created using VMD⁶⁵ or PyMOL.⁶⁷

RESULTS

Conformational sampling

To monitor protein stability and analyze the amount of conformational sampling obtained in the simulations we (1) computed monomer and TMD C α RMSDs after least square fitting to the X-ray structure [Fig. 1(b, c)]; (2) performed a principal component analyses of the TMD C α atoms [Fig. 1(d)]; and (3) calculated for each monomer in each run the distribution of χ_1/χ_2 dihedrals of all TMD residues interacting with monomer B-internal water to assess the sampling of side chain conformations (Supporting Information Fig. S1). After 50 ns, monomer RMSDs range from 2.2 to 3.4 Å [Fig. 1(b)] and although the conformational drift away from the crystal structure slows down during the simulations, on monomer level no RMSD plateau is reached. On TMD level the RMSD range extends from 1.7 to 2.8 Å except for two simulations where end RMSDs of 2.9 and 3.2 Å are reached [Fig. 1(c)] due to a shift of the cytoplasmic loop connecting trans-membrane helix 6 and helix 1 α 2 in monomer A run, after 25 ns all TMD RMSD curves have reached a plateau. As indicated by the principal compo-

nent analyses [Fig. 1(d)], all six simulations sample different regions of conformational space. The RMSD between the respective mean structures ranges from 2.1 to 2.5 Å. Although the χ_1/χ_2 dihedrals distribution is different for each monomer, all six runs yield similar χ_1/χ_2 patterns within the same monomer (Supporting Information Fig. S1).

Water in the trans-membrane domain

To determine the TMD-internal water distribution and dynamics, we computed for each monomer water residence probabilities in form of mean water densities^{32,33} using four different time windows of 50, 25, 16.7, and 5 ns. Except for the latter the water densities were averaged over all six simulations.

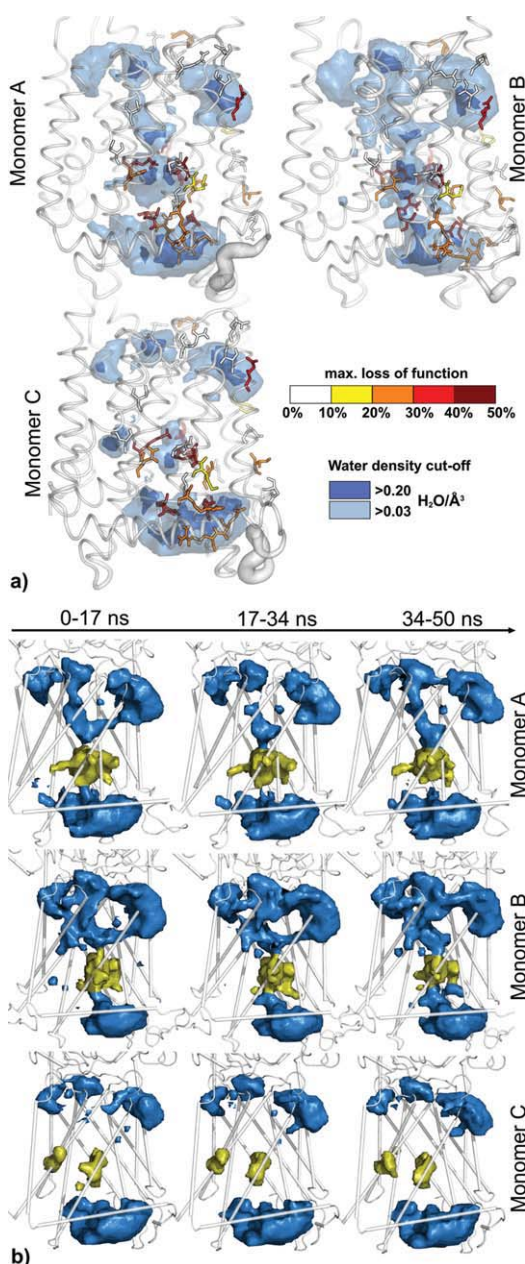
Organization

As shown in Figure 2(c,d), TMD-internal water is organized into six sections: (1) periplasmic bulk water, (2) up to three periplasmic channels E1-3 leading into the TMD, (3) a conflux region (CF) where the entry channels merge into one, (4) one centrally located core region (CR), and (5) a cytoplasmic channel X connecting to (6) cytoplasmic bulk water. The core region includes the experimentally known proton transfer key residues Asp407, Asp408, Lys940, and Thr978 and is permanently hydrated by a group of up to 12 water molecules. The residues lining water channels, conflux, and core region are summarized in Table I.

Figure 3(a) shows the run-averaged water densities calculated over the entire 50 ns simulation time (transparent isosurfaces) in context with 15 experimentally tested TMD residues and their maximum impact on AcrB function.^{38,40,41} Whereas in monomer B CF, CR and all four water channels are present, in monomer A the only connection between CF/CR and bulk water is provided by E2. In monomer C, only the CR water density is observed, split in two separate water densities and isolated from bulk water. Preferred hydration sites - opaque isosurfaces enveloping mean water densities exceeding 0.2 H₂O/Å³ are found at the beginnings of E1-3, in the conflux region, the core region, in the cytoplasmic bulk water, as well as near the X channel in monomer B. The experimentally tested residues display a correlation between a point mutation’s influence on AcrB function and a residue’s location in respect to the water densities. Whereas high impact residues cluster in the core region and the X channel, residues with lesser impact are located at the periplasmic water channels or in areas without any contact to TMD-internal water.

Dynamics

To test if the TMD hydration pattern is constant or dynamic within each monomer, we increased the time

**Figure 3**

Water distribution in the TMDs represented as run-averaged mean water densities computed over the entire 50 ns (a) and time windows of 16.7 ns (b). (a) Additionally shows 15 experimentally tested residues and their influence on AcrB function. Whereas the core region (yellow) is continuously hydrated in all monomers, connections to bulk water are only present in monomers A and B. When time resolution is increased and water densities are calculated over thirds of simulation time, it becomes evident that in monomer A and B the TMD hydration pattern is dynamic (b). Except for opaque isosurfaces in (a) indicating preferred hydration sites with water densities $>0.2 \text{ H}_2\text{O}/\text{\AA}^3$, all other isosurfaces represent water densities exceeding $0.03 \text{ H}_2\text{O}/\text{\AA}^3$. The protein conformations shown are monomer average structures with the root mean square fluctuations represented as tube thickness in (a).

resolution computing run-averaged water densities over thirds of simulation time. As shown in Figure 3(b), in monomer A and B the TMD hydration pattern is dynamic. Whereas in monomer A [Fig. 3(b), upper row] E2 and E3 are present during the first (0–17 ns) and absent during second third (17–34 ns) of the simulations, E2 reappears in the last third (34–50 ns). Connecting the core region with the cytoplasmic bulk water and passing by the 5th known key residue Arg971, the X channel is present during the first, but not in the last two thirds of the trajectory. Except for E3 disappearing in the last third of the trajectories in monomer B, X and E1-3 are observed throughout the entire simulation time connecting the core region with the periplasmic and cytoplasmic bulk phase [Fig. 3(b), middle row]. Monomer C [Fig. 3(b), bottom row] shows the same hydration pattern as in the 50 ns analysis.

To quantify the opening and closing behavior of the water channels, we increased the time resolution to 5 ns, and computed for each monomer the water densities in each of the six simulations (Supporting Information Figs. S2). A channel was considered open when containing water for at least half of the 5 ns observation time which we found corresponding to mean water density of at least $0.2 \text{ H}_2\text{O}/\text{\AA}^3$. As summarized in Table II, each channel opens and closes randomly and except for a single event in monomer B where E2 and E3 are simultaneously open for 10% of the simulation time in monomer B during run 6, only one periplasmic channel is open at the same time. On the basis of their maximum opening times the water channels rank in an order of E2 (0–50%) > X (0–30%) > E3 (0–10%) in monomer A, and E2 (0–100%) > X (0–90%) > E1 (0–70%) > E3 (0–60%) in monomer B. In monomer C all water channels are closed.

To test if the transient bulk water connections provided by the E1-3 and X channels lead to a preferred direction of water flow, we monitored the Z coordinate of all water molecules found at least once inside the conflux or core region (Fig. 4, Table III). As represented in Figure 4, we observe two types of H₂O movements. Water molecules either enter and leave the TMD on the same side (Fig. 4, orange and green) or traverse the TMD from periplasm to cytoplasm (Fig. 4, red) or vice versa (Fig. 4, blue). Whereas TMD crossings were only observed 7 and 8 times, entering and leaving the TMD on the same side is the predominant type of water motion in all simulations (Table III). No preferred direction of water flow is observed.

Inside the channels, we observe TMD water either diffusing randomly or transiently forming strings of hydrogen-bonded water molecules as illustrated by representative monomer A and B simulation snapshots in Figure 5. Such water wires do not span the entire distance between bulk water phases but occur between distinctive way points providing temporary connections between: (I) periplasmic bulk water and the conflux region via each

Table II

Opening States of the Cytoplasmic (X) and Periplasmic (E1–3) TMD Water Channels

	MD 1				MD 2				MD 3				MD 4				MD 5				MD 6				
	X	E1	E2	E3	X	E1	E2	E3	X	E1	E2	E3	X	E1	E2	E3	X	E1	E2	E3	X	E1	E2	E3	
Chain A																									
0–5 ns	0	–	–	–	0	–	–	–	–	–	–	–	–	–	–	–	–	–	–	–	–	–	0	–	
5–10 ns	0	–	–	–	–	–	–	–	–	–	–	–	0	–	–	–	–	–	–	–	–	–	–	–	–
10–15 ns	0	–	–	–	–	–	–	–	–	–	–	–	–	–	–	–	–	–	–	0	–	–	–	–	
15–20 ns	–	–	–	–	–	–	–	–	–	–	–	–	–	–	–	–	–	–	–	–	–	–	–	–	
20–25 ns	–	–	–	–	–	–	0	–	–	–	–	–	–	–	–	–	–	–	–	–	–	–	–	–	
25–30 ns	–	–	–	–	–	–	–	–	–	–	–	–	–	–	–	–	–	–	–	–	–	–	–	–	
30–35 ns	–	–	–	–	–	–	0	–	–	–	–	–	–	–	–	–	–	–	–	–	–	–	–	–	
35–40 ns	–	–	–	–	–	–	0	–	–	–	–	–	–	–	–	–	–	–	–	–	–	–	–	–	
40–45 ns	–	–	–	–	–	–	0	–	–	–	–	–	–	–	–	–	–	–	–	–	–	–	–	–	
45–50 ns	–	–	–	–	–	–	0	–	–	–	–	–	–	–	–	–	–	–	–	–	–	–	–	–	
Open	30%	0%	0%	0%	10%	0%	50%	0%	0%	0%	10%	0%	0%	0%	0%	0%	10%	0%	0%	10%	0%	0%	10%	0%	
Chain B																									
0–5 ns	–	–	0	–	0	0	–	–	–	–	–	–	–	–	–	–	–	–	–	–	–	–	0	0	
5–10 ns	–	–	0	–	–	0	–	–	–	–	0	–	–	–	0	–	–	0	–	–	0	–	–	–	
10–15 ns	0	–	0	–	–	–	–	–	–	0	–	–	–	0	–	–	0	–	0	–	0	–	–	–	
15–20 ns	–	–	0	–	–	0	–	–	–	0	–	0	–	0	–	–	–	–	–	0	–	–	–	–	
20–25 ns	–	–	0	–	–	0	–	–	–	0	–	0	–	0	–	0	–	–	0	–	–	0	–	–	
25–30 ns	–	–	0	–	–	–	–	0	–	0	–	0	–	0	–	–	–	–	–	0	–	–	–	–	
30–35 ns	–	–	0	–	–	0	–	–	0	–	0	–	0	–	0	–	–	0	–	–	0	–	–	–	
35–40 ns	–	–	0	–	–	–	–	0	–	0	–	0	–	0	–	–	0	–	–	0	–	–	–	–	
40–45 ns	–	–	0	–	–	0	–	–	0	–	0	–	0	–	0	–	–	0	–	–	0	–	–	–	
45–50 ns	–	–	0	–	–	0	–	–	0	–	0	–	0	–	0	–	–	0	–	–	0	–	–	–	
Open	10%	0%	100%	0%	10%	70%	0%	0%	40%	0%	0%	60%	0%	30%	0%	0%	70%	0%	0%	10%	0%	90%	0%	10%	0%

A channel was considered open (O) when containing water molecules for at least half the time of each 5 ns observation time window. The underlying water densities this table is based on are shown in Supporting Information Figures S2–S4.

of the E1–3 channels—though not simultaneously [Fig. 5(a–c)]; (II) conflux and core region [Fig. 5(d)]; and (III) core region and cytoplasmic bulk water via the X channel [Fig. 5(e)]. Whereas these water wire configurations occur frequently throughout the simulations, a direct connection between core region and periplasmic bulk water bypassing the conflux region was observed only four times in monomer B [Fig. 5(f)].

Residue water interaction

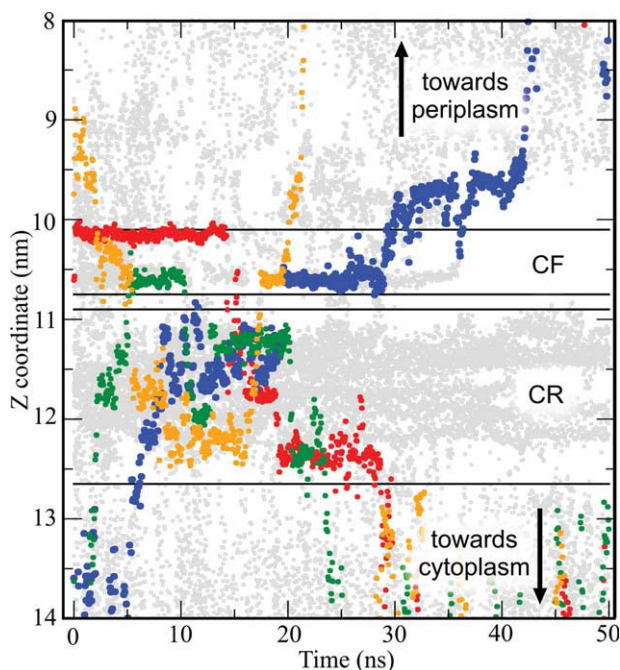
The results of the hydrogen bond analysis are described in the Supporting Information material (Supporting Information results, Supporting Information Table S2 and Figs. S5–S6). Whereas in monomer B and C the five key residues display a similar side chain orientation as in the crystal structure, Lys940 undergoes a tilting motion in monomer A shifting away by 6.6 Å (N ζ -N ζ distance) from its x-ray conformation (Supporting Information Fig. S7).

Regulation of TMD water access

To elucidate how TMD water access is regulated, we performed a two-step analysis (Fig. 6). First we superimposed and compared the TMD average structures of monomer B and C as they represent extremes of TMD hydration in our simulations (Fig. 3, Supporting Information Figs. S2–S4, Table II). In a second step we

inspected the regions on the outer protein surface lining the mouths of the water channels and containing residues of key residue-like H-bond frequencies (Supporting Information Table S2, Fig. S6). We find that TMD water access is regulated in a combination of monomer-specific shifts of trans-membrane helices (Fig. 6, left column) and side-chain reorientations of four groups of residues (Fig. 6, middle and right column, Table I).

On periplasmic side the E1 channel is regulated by a ~9 Å movement of the middle part of helix 8 towards helices 10 and 9 [Fig. 6(a), left column], which results in Tyr877 blocking the passage of water molecules [Fig. 6(a) middle and left column]. In the closed state the Tyr877 conformation is stabilized by hydrogen bond interaction either with Asn923, Gln928, or Ser561, which along with Phe556, Phe927, Leu931, and Val908 form the first group of gating residues [Fig. 6(a)]. Closure of E2 is caused by the upper periplasmic parts of helices 9 and 12 approaching each other [Fig. 6(b), left column]. At the same time E2 is sealed by the second group of gating residues comprising Thr1005, Ala1002, Leu921, Phe927, Gly930, Gly1006, and Leu931 [Fig. 6(b), middle and right column]. E3 closure is due to a movement of helix 11 towards helix 2 and 4 [Fig. 6(c), left column] and the third group of gating residues: Leu989, Ser988, Val986, The343, Gly985, Glu346, Ala347, Leu350 [Fig. 6(c), middle and right column]. On cytoplasmic side the X channel is closed by helix 5

**Figure 4**

As represented by Z-coordinate trajectories of water molecules found inside one monomer in a single MD run, two types of water movements occur in the TMDs throughout the simulations. Water molecules either traverse the TMD (blue and red) or enter and leave the TMD on the same side (orange and green). As indicated by the results of the water flow analysis of each monomer and each MD run (Table III), entering and leaving on the same side is the predominant type of TMD water movement in our simulations.

shifting towards the TMD's geometrical center [Fig. 6(d), left column]. When X is sealed, residues Leu442, Val411, Ile975, Leu944, and Pro974 form a hydrophobic barrier blocking water molecules and keeping Arg971 from adopting a core region-facing orientation [Fig. 6(d), middle column]. In the open conformation [Fig. 6(d), right column], the exit passage is widened by $\sim 10 \text{ \AA}^2$ (approximated by differences in the triangular area spanned by Leu442, Leu944, and Val411) and the side-chain of Arg971 orients towards the now accessible polar residues in the core region followed by an influx of water molecules. In contrast to monomer C where no exchange with bulk water occurs, water channels open and close in monomers A and B. Here, water access is mainly regulated by side-chain re-orientations. Supporting Information Figure S8 additionally shows the location of the gating residues in relation to the phospholipid head groups.

DISCUSSION

In this study we have analyzed the water distribution in the AcrB trans-membrane domains, determined new key residue candidates, and identified possible pathways of proton conduction. This was done analyzing TMD-

water dynamics and residue interaction, obtained in a series of $6 \times 50 \text{ ns}$ independent MD simulations of asymmetric and substrate-free AcrB¹⁵ embedded in a phospholipid/150 mM NaCl environment simulating the protonation scenario proposed in Reference 17. We begin this section discussing the limitations of our approach and then proceed to our findings and their possible biological implications.

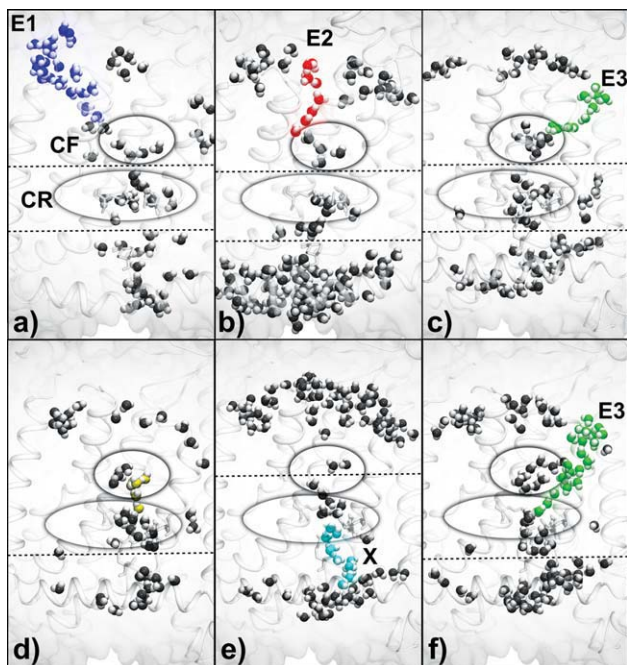
Limitations of our approach

Because molecular topologies are usually constant during standard MD, the use of classical molecular dynamics simulations to investigate intra-protein proton transport might raise the question of an adequacy of method. Whereas the explicit simulation of proton transfer is indeed not possible via standard MD, requiring full or at least partial quantum mechanical treatment,^{27,45–50} the situation is different when the focus is on the dynamics of water in the protein interior at a given protonation state. Like water positions in an X-ray structure provide clues to possible routes of proton transfer, molecular dynamics simulation can extend this information by providing a more complete representation of the overall protein hydration adding the element of dynamics. Whereas crystal waters often represent only the subset of firmly coordinated water molecules, solvation in an MD simulation is cavity analysis-based yielding full hydration where sterically possible. Throughout an MD simulation water molecules can dynamically probe the available space yielding a more accurate representation of the protein-internal water distribution which include the diffusion of misplaced water molecules out of energetically un-favored environments.^{54,66} Recent examples of this MD approach to proton transfer include studies on bacteriorhodopsin^{32,33} or the sodium/proton antiporter NhaA.³⁰

Table III

Number of Water Molecules Entering and Leaving the Trans-Membrane Domains

MD	Monomer	Cytoplasm		Periplasm		Crossings	
		Entering from	Leaving to	Entering from	Leaving to	to cytoplasm	to periplasm
1	A	28	34	16	17	0	0
	B	84	82	200	202	1	0
2	A	131	135	509	506	0	0
	B	14	15	100	98	0	0
3	A	21	24	153	158	0	0
	B	60	57	395	404	0	4
4	A	17	18	51	56	0	0
	B	51	54	120	123	0	0
5	A	11	12	40	47	0	1
	B	40	43	24	28	1	0
6	A	5	5	42	46	0	0
	B	40	84	147	151	5	3

**Figure 5**

TMD water transiently forms strings of hydrogen-bonded water molecules. As illustrated by representative simulation snapshots from monomer B (a, c–f) and A (b), these water wires provide temporary connections between periplasmic bulk water and the conflux region CF via each of the three entry channels E1–3 (a–c), conflux and core region (CR) (d) as well as between core region and cytoplasmic bulk water via the exit channel X (e). Whereas the water structures in a–e occur frequently throughout the simulation, a direct connection between core region and periplasmic bulk water bypassing the conflux region was only observed four times in monomer B (f). Dotted lines indicate no hydrogen bond contact between water clusters.

Controlling side chain conformations and water distribution, protonation states of key residues are crucial for proton transporting systems. For AcrB, monomer-specific protonation states have been proposed for Asp407, Asp408, Lys940, Arg971 based on their crystal structure conformations.¹⁷ Although it would be desirable having the protonation states of proton transfer-relevant residues further investigated experimentally, for example, by infrared spectroscopy, in this study we explore protein and water dynamics based on the hypothesis that only four residues change protonation state throughout the reaction cycle¹⁷ while standard protonation states apply for all other titratable residues. As it is currently unknown if this list of protonation-changing residues is complete, our study should be seen as a first simulation attempt to assess the dynamical consequences arising from that particular protonation scenario reflecting the current state of AcrB knowledge. As the motif of two deprotonated side chain carboxyl groups immediately facing each other is a known characteristic of the proton release group in another proton pump^{68,69} we have scanned for aspartates and glutamates in a similar ori-

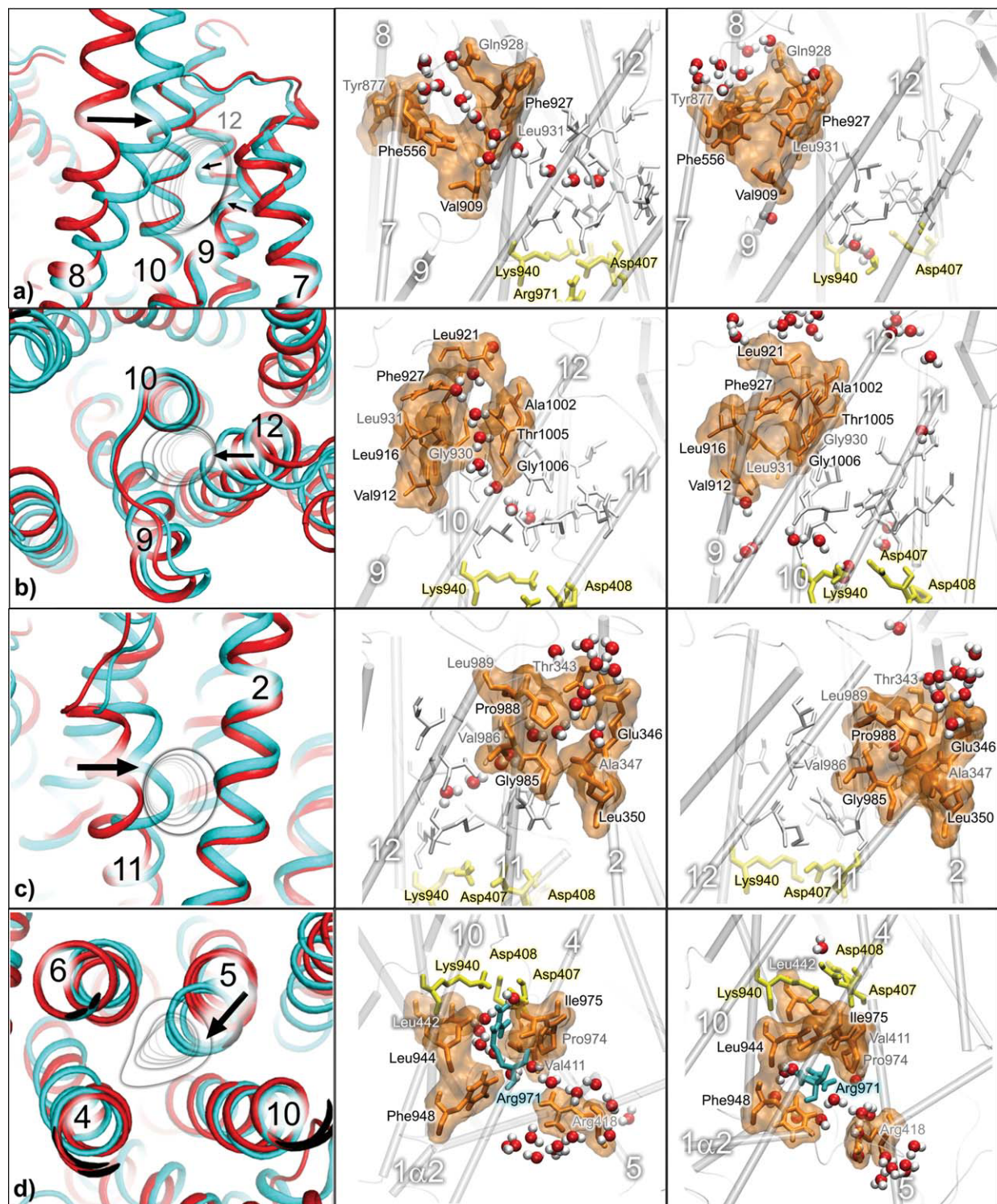
entation in AcrB. No such pairing was found which might suggest a different mechanism of proton release.

As simulation time is naturally limited, the question always arises whether a simulation is long enough. The answer depends on the problem under investigation. In this study, we address the question of the internal hydration of the proton-conducting subunit of transport protein. Protein-internal water distribution is to a large degree influenced by water diffusion and the protein structure – both on a level of tertiary structure and side chain conformations of residues interacting with internal water molecules. Whereas the tertiary structure of the entire AcrB subunits has expectedly⁷⁰ not equilibrated after 50 ns [Fig. 1(b)], the TMD subunits reach RMSDs plateaus within 25 ns in 5 out of 6 runs [Fig. 1(c)]. Although an RMSD plateau is a necessary but not sufficient condition for structure convergence, principal component analysis can provide more detailed information on conformational sampling.⁷⁰ Although during the 300 ns of total production run simulation time each of the six independent 50 ns runs sampled different regions of conformational space [Fig. 1(d)], the resulting TMD average structures are not further apart than 2.5 Å. Beyond that the largest root mean square fluctuation in the run-averaged monomer structures concentrate on cytoplasmic loop regions [Fig. 3(a)]. As indicated by the distribution of the χ_1/χ_2 dihedrals of residues interacting with TMD-internal water (Supporting Information Fig. S1), whereas different side chain conformations were sampled in each monomer, each run sampled similar side chain conformations within the same monomer. Furthermore, given the self-diffusion speed of water under the simulated conditions,^{71,72} we consider it reasonable to assume that 50 ns is long enough to at least permit water molecules to sufficiently sample the AcrB TMD interior in near X-ray conformations (Figs. 2 and 3, Supporting Information Figs. S2–S4 and S6). The high degree of water exchange we observe during the simulations (Fig. 4, Table III) also supports this assumption. Beyond that, similar work on bacteriorhodopsin yielded insightful results on a simulation time scale that was 10 times shorter.^{32,33}

Two further simplifications of our simulations that should be kept in mind concern the lipid environment of AcrB represented by a homogeneous POPE bilayer and the neglect of any other interaction partners like AcrA, TolC, or YajC.^{73–76} Whereas the former is a common approximation in simulating bacterial membrane proteins that is justified by a natural occurrence of 75–85% POPE in the *E. coli* membranes,⁷⁷ simulations assessing the influence of other AcrB interaction partners and protonation states are currently under way in our lab.

Asymmetric water distribution

As reflected by the mean water densities, the distribution of TMD-internal water is different in each monomer

**Figure 6**

TMD water access is regulated by four groups of residues in a combination of side chain re-orientations (middle and right column) preceded by monomer-specific shifts of trans-membrane helices (left column). The gating residues are located at the beginnings of the periplasmic entry channels E1-3 (**a–c**) and the cytoplasmic exit channel X (**d**). Whereas middle and right columns show the gating residues (orange) in open and closed conformation, the left column highlights the involvement of helix shifts illustrated by the super-imposed average conformations of monomer B (red) and C (cyan). Black arrows mark helix shifts, gray lines indicate the outer entrances of the water channels.

(Figs. 2 and 3, Supporting Information Figs. S2–S6). While periplasmic and cytoplasmic water phases are on average connected transiently in monomer A and throughout the entire simulation time in monomer B, no such connection exists in monomer C. Furthermore, with the exception of monomer C, TMD hydration is also asymmetric within each monomer with up to three periplasmic water channels E1-3 but only a single cytoplasmic channel X connecting core and conflux region to bulk water. Given that monomer asymmetry is one of the key characteristics of the AcrB trimer,^{14–16} it is not surprising to see asymmetry also on the level of TMD hydration. The monomer-specific pattern of bulk water accessibility is also compatible with some of the currently postulated functional mechanisms of AcrB proton transport,^{17,78,79} which we will discuss in detail below. While the key residue-encompassing core region is continuously hydrated throughout the three intermediates (Fig. 3, 4, Supporting Information Figs. S2–S4, S6, it separates into at least two water clusters in monomer C (Fig. 3, Supporting Information Figs. S4, S6) due to a size reduction of the original cavity and the appearance of a secondary cavity not present in A or B. With Lys940 deprotonated, Asp407 and Asp408 protonated and Arg971 facing towards cytoplasmic bulk water, this could be a consequence of the absence of any charged residues in monomer C's core region (Fig. 7, Table I). Furthermore the separate water clusters could also suggest that a constant influx of water molecules is necessary to stabilize a single coherent water cluster.

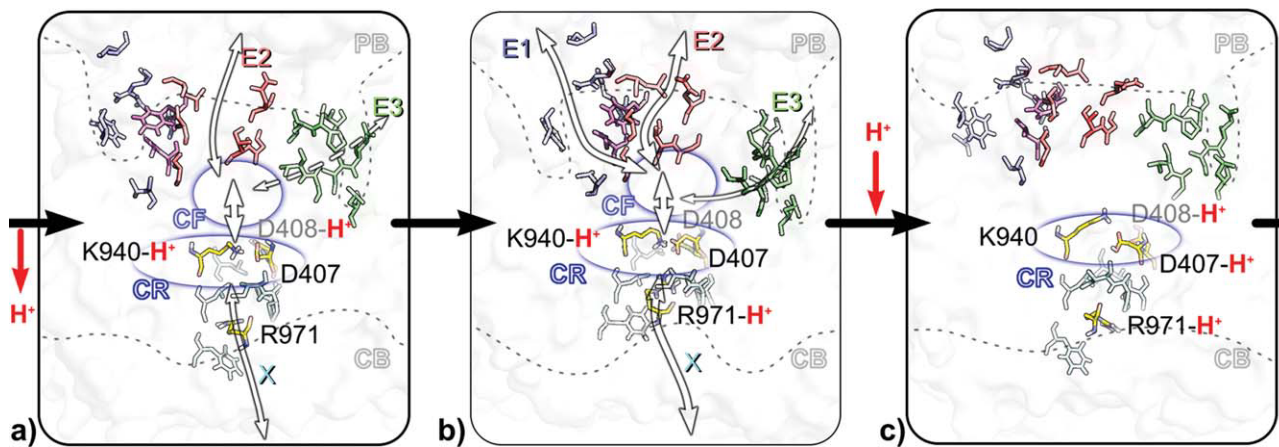
Three routes for proton transfer

Do the three periplasmic and the single cytoplasmic water channels represent likely routes for proton transfer? The assumption seems reasonable given (a) how the water channels provide connections between known key residues and bulk water (Fig. 3, Supporting Information Figs. S2–S4, S6, Table II), (b) the occurrence of proton wire-like water structures⁸⁰ in these connections (Fig. 5), and (c) the monomer- and therefore intermediate-specific patterns of water distribution and residue interaction (Fig. 3, Supporting Information Figs. S2–S6, Table S2). Against this backdrop our findings partially confirm the model of two half channels of proton transport⁷⁸—however, our data suggests that the periplasmic half channel is branched into three channels accessing bulk water. The putative presence of three different ways connecting periplasm to the key residue-encompassing core region might suggest that a simultaneous blocking of all three routes is necessary to prevent AcrB proton transport activity. Multiple proton entry routes would also explain the little or no effect on AcrB activity observed in mutation studies of Thr343, Glu339, Gln1000, and Thr993.⁴¹ Located all along the E3 channel mutation of these residues leaves

the other two entry channels intact [Fig. 3(a)]. Conversely, in light of our findings, mutagenesis studies removing or adding bulky residues in all three entry channels should show a greater effect on AcrB activity. Concerning possible modes of proton conduction, our findings suggest two possible means of transport: either diffusion of an individual hydronium ion or larger protonated water cluster or more rapid proton transfer along proton wires transiently connecting bulk water, conflux, and core region (Fig. 5).

Properties of known key residues

Five key residues of proton conduction have been determined in mutagenesis experiments whose replacement with alanine leads to a loss in AcrB activity of 90% or more.^{13,38–41} Our simulation data provide some new insight into the molecular details characterizing a key residue. Except for Arg971, key residues line or are embedded in the only stable water cluster in the TMD core region (Figs. 2(d), 3, Supporting Information Fig. S6) suggesting that permanent hydration here is crucial. This could be further explored simulating alanine mutants of each key residue to study its effect on the core region hydration. Such simulations are currently underway in our lab. For Arg971 on the other hand, the current wild type simulations already provide a possible explanation of its special role. Switching between orientations facing towards or away from the core region (Fig. 6(d), 7) Arg971 mediates water access and exchange between core region and cytoplasmic bulk water depending on the gating residue conformation in this region [Fig. 6(d)]. Additionally, its direct contact with the cytoplasmic bulk phase in monomer C (Fig. 7) supports the hypothesis that Arg971 is a likely candidate for the proton release group.⁴⁰ Although four key residues are in the core region, only Asp407 is always in water hydrogen bond contact [Supporting Information Fig. S5(a–c), Table S2]. The other key residues show a heterogeneous pattern of H-bond water interaction that is different from monomer to monomer (Supporting Information Table S2). Whereas Asp408 and Lys940 have the least water contact in monomer C, Arg971, and Thr978 have the least water contact in monomer A where hydrogen bonds are predominantly formed with Arg418 and Asp407, respectively. Apparently a continuously high water H-bond contact frequency is not an exclusive characteristic of AcrB key residues. Whereas in monomer B and C the key residues display a similar orientation and conformation as in the crystal structure,¹⁵ we observe deviating conformations in monomer A. With Lys940 shifting away by 6.6 Å from its X-ray orientation (Supporting Information Fig. S7), this could be interpreted as either the molecular representation used in our simulations is incomplete or the assumed protonated state of Asp408 in monomer A is incorrect. The latter possibility is also

**Figure 7**

Water accessibility and protonation states during the AcrB reaction cycle. Two residue-bound excess protons in the A and B intermediates (a,b) and three in C (c) suggest that proton uptake and release occur during the transition from B to C and C to A, respectively. Our simulation data indicates that bulk phase-accessing water diffusion pathways, along which protons could travel, are present only in A and B suggesting two possible scenarios for proton uptake: either during a so far unknown intermediate between B and C where periplasmic bulk water (PB) access is still given; or during the A or B intermediate where the third excess proton is transiently stored in a water cluster of the conflux (CF) or core region (CR) and does not become residue-bound until the c intermediate is reached. For proton release a hydrated exit channel X is not required as protonated Arg971 is already in contact with cytoplasmic bulk water (CB) in C. Dotted lines indicate bulk water range, whereas dotted, thin and bold white arrows indicate water diffusion pathways where run-averaged water densities were observed for 33%, 66%, or 100% of simulation time. Residue conformations are taken from representative simulation average structures, which are simulation snap shots whose overall RMSD to the actual average structure is minimal.

supported by crystallographic studies suggesting that Asp408 might be deprotonated in A.⁴⁰

In addition to the five key residues, ten other residues have been tested experimentally^{38,40,41} impacting AcrB function in different ways. All tested residues show a correlation between a point mutation's influence on protein function and residue location in context of the TMD water distribution [Fig. 3(a)]. Whereas high impact residues cluster in the core region and the X channel, residues with lesser impact are located at the periplasmic water channels or in areas without any contact to with TMD-internal water. Next to providing supporting evidence for the veracity of our predicted water distributions, this also suggests that (a) high impact residues affect TMD hydration and (b) this effect is more pronounced when point mutations are introduced into unique sections of the water distribution for which—unlike the three periplasmic entry channels—no alternate water routes exist. The little effect of the Thr933 mutant in the conflux region could be explained by water molecules mainly coordinated by the protein backbone atoms whereas 88% maximum loss of function of Glu414 replacement could imply a potential involvement in proton release.

New candidates

Combining the information of TMD hydration (Figs. 3 and 5, Supporting Information Figs. S2–S4 and S6), water-interacting residues (Supporting Information Figs.

S5–S6, Table S2) and conformational changes between monomers (Fig. 6), we identified three groups of new putative key residue candidates. (I) Lining the mean water densities, framework residues provide the structural scaffold for TMD water organization into three periplasmic channels, one conflux region, one core region and one cytoplasmic channel [Figs. 2(c,d) and 3, Table I]. (II) Located at the mouths of the E1-3 and X channels (Fig. 6, Table I), gating residues are essentially a subset of framework residues that regulate TMD hydration through side chain re-orientations once a monomer has been “activated.” The activation involves monomer-specific shifts of α -helices inducing a transition from a state without bulk water access as in monomer C, to a state where the water channels open and close randomly as in monomers A and B (Supporting Information Figs. S2–S4, Table II). If our findings are correct both framework and gating residues could be tested using AcrB mutants that either cut off core region water supply or disable water access regulation by introducing or removing bulky residues in the gating regions or the conflux region. Shifts of trans-membrane helices could be detected by linear dichroism spectroscopy. (III) Detected by a homogenous Asp407-like hydrogen bonding pattern (Supporting Information Table S2), we propose Glu339, Glu346, and Asp924 on the periplasmic TMD surface to act as proton antennas based on three observations: (1) negatively charged surface residues in H⁺-transporting proteins are known to attract protons directing them towards the proton conduction channel.⁸¹ (2) Located at

the mouths of E2 and E3, Glu339, Glu346, and Asp924 are the only negatively charged residues on the periplasmic TMD surface. (3) Mutation of Glu339 was reported to have little effect on MexB activity unless a positively charged residue was introduced leading to an activity loss of 50–75%.³⁸ While channel-flanking proton antennas on the periplasmic surface seem a plausible hypothesis that could be readily tested by a simultaneous replacement with arginine or lysine, the question arises why two antennas should be flanking the E3 entrance when there is only one for E2 and apparently none for E1. One possible explanation regards the location of the channel mouths in respect to the lipid head groups. Whereas E1 and E2 are situated at head group level, the E3 mouth is located 13 Å below the POPE head groups (Supporting Information Fig. S8). Unless the POPE topology used in this study is completely incorrect, it is understandable that E3 requires more negatively charged residues to attract waters and protons below the lipid head groups. Located at head group level, one proton antenna would be sufficient for E2, whereas E1 might share the Asp924 antenna with E2 given the close proximity of both entrances (Fig. 7).

Implications for proton transfer

On the basis of crystallographic data, the current AcrB protonation scenario proposes two residue-bound excess protons in the A and B intermediate and three in C.¹⁷ Proton uptake has been postulated to occur either in B,⁷⁹ during the transition from B to C¹⁷ or in C.⁷⁸ Proton release has been proposed taking place during the C^{17,79} or the A intermediate.⁷⁸ Additional proton uptake and release events are anticipated but require further structural data to be elucidated.⁷⁹ Our simulation data indicate that bulk phase-accessing water diffusion pathways, along which protons could travel, are present in the A and B intermediates but not in C (Fig. 7). Ruling out a proton uptake from bulk water in C, two possible scenarios seem plausible: (I) Similar to¹⁷ proton uptake could occur during a so far unknown intermediate between B and C where periplasmic bulk water access is still given. (II) Entering the TMD already during the A or B intermediate,⁷⁹ the third excess proton is transiently stored in a water cluster and does not become residue-bound until the C intermediate is reached. Likely locations for such a water cluster would be conflux or the continuously hydrated core region. If the second hypothesis is correct and the proposed protonated water cluster is sufficiently long-lived, its continuum absorbance bands⁸² could be detected by infrared spectroscopy. For proton release our simulations suggests that a hydrated cytoplasmic channel X is not required because protonated Arg971 is already in contact with cytoplasmic bulk water in monomer C, supporting a deprotonation of the arginine either in C^{17,79} or during the transition to A.

Whether the excess proton then immediately leaves the TMD or is transiently bound to other TMD residues such as Glu414, Glu417, Arg418, Arg973 cannot be deduced from the currently available data.

CONCLUSIONS

We have performed 6×50 ns molecular dynamics simulation of membrane-embedded, asymmetric AcrB to address the questions of trans-membrane domain hydration, possible routes of proton transfer and new key residue candidates. Simulating each monomer in its proposed protonation state, we calculated for each trans-membrane domain the average water distribution, identified residues interacting with these waters and quantified each residue's frequency of water hydrogen bond contact. We find three possible routes of proton transfer characterized by an always hydrated and key residue-encompassing core region present in all monomers that is continuously connected to bulk water in monomer B and transiently in A by one cytoplasmic and up to three periplasm water channels. We find that water access of the trans-membrane domains is regulated by four groups of residues in a combination of side chain re-orientations preceded by shifts of trans-membrane helices. Our findings support a proton release event via Arg971 during the C intermediate or in the transition to A, and proton uptake occurring either in the A or B state or during a so far unknown intermediate in between B and C where cytoplasmic water access is still possible. Complementing and providing a better understanding of some of the known experimental data, our simulations also suggest experimentally testable hypotheses, which have not been investigated so far.

ACKNOWLEDGMENTS

The authors thank Martin Raunest for his help in processing the water densities as well as Drs. Frank Wennmohs, Tim Harder, and Prof. Dr. Jürgen Bajorath for proof reading and helpful comments. This work was financially supported by the Ministerium für Innovation, Wissenschaft, Forschung und Technologie des Landes Nordrhein-Westfalen. ChK is a junior research group leader funded by the NRW Rückkehrerprogramm.

REFERENCES

1. Summers WC. Microbial drug resistance: a historical perspective. In: Bacterial resistance to antimicrobials, Vol. 2. CRC Press; 2008. pp 1–9.
2. Nikaido H. Multidrug resistance in bacteria. Annu Rev Biochem 2009;78:119–146.
3. Saier MH, Jr, Paulsen IT. Phylogeny of multidrug transporters. Semin Cell Dev Biol 2001;12:205–213.
4. Ma D, Cook DN, Alberti M, Pon NG, Nikaido H, Hearst JE. Molecular cloning and characterization of acrA and acrE genes of Escherichia coli. J Bacteriology 1993;175:6299–6313.

5. Lomovskaya NY, Zgurskaya H, Bostian KA, Lewis K. Multidrug efflux pumps: structure, mechanism, and inhibition. Bacterial resistance to antimicrobials. CRC Press; 2008. pp 45–70.
6. Zgurskaya HI, Nikaido H. Bypassing the periplasm: reconstitution of the AcrAB multidrug efflux pump of *Escherichia coli*. *Proc Natl Acad Sci USA* 1999;96:7190–7195.
7. Zgurskaya HI, Nikaido H. AcrA is a highly asymmetric protein capable of spanning the periplasm. *J Mol Biol* 1999;285:409–420.
8. Nikaido H. Antibiotic resistance caused by gram-negative multidrug efflux pumps. *Clin Infect Dis* 1998;27 (Suppl 1):S32–S41.
9. Nikaido H. Multidrug efflux pumps of gram-negative bacteria. *J Bacteriology* 1996;178:5853–5859.
10. Piddock LJV. Clinically relevant chromosomally encoded multidrug resistance efflux pumps in bacteria. *Clin Microbiol Rev* 2006; 19:382–402.
11. Tikhonova EB, Zgurskaya HI. AcrA, AcrB, and TolC of *Escherichia coli* form a stable intermembrane multidrug efflux complex. *J Biol Chem* 2004;279:32116–32124.
12. Zgurskaya HI, Nikaido H. Cross-linked complex between oligomeric periplasmic lipoprotein AcrA and the inner-membrane-associated multidrug efflux pump AcrB from *Escherichia coli*. *J Bacteriology* 2000;182:4264–4267.
13. Murakami S, Nakashima R, Yamashita E, Yamaguchi A. Crystal structure of bacterial multidrug efflux transporter AcrB. *Nature* 2002;419:587–593.
14. Murakami S, Nakashima R, Yamashita E, Matsumoto T, Yamaguchi A. Crystal structures of a multidrug transporter reveal a functionally rotating mechanism. *Nature* 2006;443:173–179.
15. Seeger MA, Schiefner A, Eicher T, Verrey F, Diederichs K, Pos KM. Structural asymmetry of AcrB trimer suggests a peristaltic pump mechanism. *Science* 2006;313:1295–1298.
16. Sennhauser G, Amstutz P, Briand C, Storchenecker O, Grutter MG. Drug export pathway of multidrug exporter AcrB revealed by DARPin inhibitors. *PLoS Biol* 2007;5:e7.
17. Seeger MA, Diederichs K, Eicher T, Brandstatter L, Schiefner A, Verrey F, Pos KM. The AcrB efflux pump: conformational cycling and peristalsis lead to multidrug resistance. *Curr Drug Targets* 2008;9:729–749.
18. Seeger MA, von Ballmoos C, Eicher T, Brandstatter L, Verrey F, Diederichs K, Pos KM. Engineered disulfide bonds support the functional rotation mechanism of multidrug efflux pump AcrB. *Nat Struct Mol Biol* 2008;15:199–205.
19. Takatsuka Y, Nikaido H. Site-directed disulfide cross-linking shows that cleft flexibility in the periplasmic domain is needed for the multidrug efflux pump AcrB of *Escherichia coli*. *J Bacteriol* 2007;189:8677–8684.
20. Zgurskaya HI. Covalently linked AcrB giant offers a new powerful tool for mechanistic analysis of multidrug efflux in bacteria. *J Bacteriology* 2009;191:1727–1728.
21. Davidson AL, Dassa E, Orelle C, Chen J. Structure, function, and evolution of bacterial ATP-binding cassette systems. *Microbiol Mol Biol Rev* 2008;72:317–364.
22. Moussatova A, Kandt C, O'Mara ML, Tielemans DP. ATP-binding cassette transporters in *Escherichia coli*. *Biochimica Et Biophysica Acta* 2008;1778:1757–1771.
23. Tamura N, Konishi S, Yamaguchi A. Mechanisms of drug/H⁺ antiport: complete cysteine-scanning mutagenesis and the protein engineering approach. *Curr Opin Chem Biol* 2003;7:570–579.
24. Nagle JF, Mille M, Morowitz HJ. Theory of hydrogen-bonded chains in bioenergetics. *J Chem Phys* 1980;72:3959–3971.
25. Buch-Pedersen MJ, Pedersen BP, Veierskov B, Nissen P, Palmgren MG. Protons and how they are transported by proton pumps. *Pflugers Arch* 2009;457:573–579.
26. Cukierman S. Et tu, Grotthuss! and other unfinished stories. *Biochim Biophys Acta* 2006;1757:876–885.
27. Marx D. Proton transfer 200 years after von Grotthuss: insights from ab initio simulations. *Chemphyschem* 2006;7: 1848–1870.
28. Wright CA. Chance and design—proton transfer in water, channels and bioenergetic proteins. *Biochim Biophys Acta* 2006;1757: 886–912.
29. Abresch EC, Paddock ML, Stowell MHB, McPhillips TM, Axelrod HL, Soltis SM, Rees DC, Okamura MY, Feher G. Identification of proton transfer pathways in the X-ray crystal structure of the bacterial reaction center from *Rhodobacter sphaeroides*. *Photosynthesis Research* 1998;55:119–125.
30. Arkin IT, Xu H, Jensen MO, Arbely E, Bennett ER, Bowers KJ, Chow E, Dror RO, Eastwood MP, Flitman-Tene R, Gregersen BA, Klepeis JL, Kolossvary I, Shan Y, Shaw DE. Mechanism of Na⁺/H⁺ antiporting. *Science* 2007;317:799–803.
31. Grudinin S, Buldt G, Gordelyi V, Baumgaertner A. Water molecules and hydrogen-bonded networks in bacteriorhodopsin—molecular dynamics simulations of the ground state and the M-intermediate. *Biophys J* 2005;88:3252–3261.
32. Kandt C, Gerwert K, Schlitter J. Water dynamics simulation as a tool for probing proton transfer pathways in a heptahelical membrane protein. *Proteins* 2005;58:528–537.
33. Kandt C, Schlitter J, Gerwert K. Dynamics of water molecules in the bacteriorhodopsin trimer in explicit lipid/water environment. *Biophys J* 2004;86:705–717.
34. Luecke H. Atomic resolution structures of bacteriorhodopsin photocycle intermediates: the role of discrete water molecules in the function of this light-driven ion pump. *Biochimica Et Biophysica Acta-Bioenergetics* 2000;1460:133–156.
35. Svensson-Ek M, Abramson J, Larsson G, Tornroth S, Brzezinski P, Iwata S. The X-ray crystal structures of wild-type and EQ(I-286) mutant cytochrome c oxidases from *Rhodobacter sphaeroides*. *J Mol Biol* 2002;321:329–339.
36. Garczarek F, Brown LS, Lanyi JK, Gerwert K. Proton binding within a membrane protein by a protonated water cluster. *Proc Natl Acad Sci USA* 2005;102:3633–3638.
37. Lanyi JK. Bacteriorhodopsin. *Annu Rev Physiology* 2004;66:665–688.
38. Guan L, Nakae T. Identification of essential charged residues in transmembrane segments of the multidrug transporter MexB of *Pseudomonas aeruginosa*. *J Bacteriol* 2001;183:1734–1739.
39. Murakami S, Yamaguchi A. Multidrug-exporting secondary transporters. *Curr Opin Struct Biol* 2003;13:443–452.
40. Seeger MA, von Ballmoos C, Verrey F, Pos KM. Crucial role of Asp408 in the proton translocation pathway of multidrug transporter AcrB: evidence from site-directed mutagenesis and carbodiimide labeling. *Biochemistry* 2009;48:5801–5812.
41. Takatsuka Y, Nikaido H. Threonine-978 in the transmembrane segment of the multidrug efflux pump AcrB of *Escherichia coli* is crucial for drug transport as a probable component of the proton relay network. *J Bacteriology* 2006;188:7284–7289.
42. Lu WC, Wang CZ, Yu EW, Ho KM. Dynamics of the trimeric AcrB transporter protein inferred from a B-factor analysis of the crystal structure. *Proteins* 2006;62:152–158.
43. Schulz R, Vargiu AV, Collu F, Kleinekathöfer U, Ruggerone P. Functional rotation of the transporter AcrB: insights into drug extrusion from simulations. *PLoS Comput Biol* 2010;6.
44. Yao XQ, Kenzaki H, Murakami S, Takada S. Drug export and allosteric coupling in a multidrug transporter revealed by molecular simulations. *Nat Commun* 2010;117.
45. Aqvist J, Warshel A. Simulation of enzyme-reactions using valence-bond force-fields and other hybrid quantum-classical approaches. *Chem Rev* 1993;93:2523–2544.
46. Kamerlin SCL, Warshel A. The EVB as a quantitative tool for formulating simulations and analyzing biological and chemical reactions. *Faraday Discussions* 2010;145:71–106.
47. Lill MA, Helms V. Molecular dynamics simulation of proton transport with quantum mechanically derived proton hopping rates (Q-HOP MD). *J Chem Phys* 2001;115:7993–8005.
48. Schmitt UW, Voth GA. Multistate empirical valence bond model for proton transport in water. *J Phys Chem B* 1998;102:5547–5551.

49. Tuckerman ME, Marx D, Klein ML, Parrinello M. On the quantum nature of the shared proton in hydrogen bonds. *Science* 1997;275:817–820.
50. Warshel A. Computer simulations of enzyme catalysis: methods, progress, and insights. *Annu Rev Biophys Biomol Struct* 2003;32:425–443.
51. Berendsen HJC, Vanderspoel D, Vandrunen R. Gromacs—a message-passing parallel molecular-dynamics implementation. *Comput Phys Commun* 1995;91:43–56.
52. Hess B, Kutzner C, van der Spoel D, Lindahl E. GROMACS 4: algorithms for highly efficient, load-balanced, and scalable molecular simulation. *J Chem Theory Comput* 2008;4:435–447.
53. Oostenbrink C, Villa A, Mark AE, van Gunsteren WF. A biomolecular force field based on the free enthalpy of hydration and solvation: the GROMOS force-field parameter sets 53A5 and 53A6. *J Comput Chem* 2004;25:1656–1676.
54. Kandt C, Ash WL, Tieleman DP. Setting up and running molecular dynamics simulations of membrane proteins. *Methods* 2007;41:475–488.
55. Pan J, Tieleman DP, Nagle JF, Kucerka N, Tristram-Nagle S. Alamethicin in lipid bilayers: combined use of X-ray scattering and MD simulations. *Biochim Biophys Acta* 2009;1788:1387–1397.
56. Berendsen HJC, Postma JPM, Vangunsteren WF, Hermans J. Interaction models for water in relation to protein hydration. In: Pullman B, editor. *Intermolecular Forces*. Dordrecht: Reidel; 1981. pp331–342.
57. Caves LS, Evanseck JD, Karplus M. Locally accessible conformations of proteins: multiple molecular dynamics simulations of crambin. *Protein Sci* 1998;7:649–666.
58. Kandt C, Tieleman DP. Holo-BtuF stabilizes the open conformation of the vitamin B12 ABC transporter BtuCD. *Proteins* 2010;78:738–753.
59. Kandt C, Xu Z, Tieleman DP. Opening and closing motions in the periplasmic vitamin B12 binding protein BtuF. *Biochemistry* 2006;45:13284–13292.
60. Hess B, Bekker H, Berendsen HJC, Fraaije JGEM. LINCS: a linear constraint solver for molecular simulations. *J Comput Chem* 1997;18:1463–1472.
61. Berendsen HJC, Postma JPM, Vangunsteren WF, Dinola A, Haak JR. Molecular-dynamics with coupling to an external bath. *J Chem Phys* 1984;81:3684–3690.
62. Darden T, York D, Pedersen L. Particle mesh ewald—an NLog(N) method for ewald sums in large systems. *J Chem Phys* 1993;98:10089–10092.
63. Essmann U, Perera L, Berkowitz ML, Darden T, Lee H, Pedersen LG. A smooth particle mesh ewald method. *J Chem Phys* 1995;103:8577–8593.
64. Henchman RH, McCammon JA. Extracting hydration sites around proteins from explicit water simulations. *J Comput Chem* 2002;23:861–869.
65. Humphrey W, Dalke A, Schulten K. VMD: visual molecular dynamics. *J Mol Graph* 1996;14:33–38,27–38.
66. Raunest M, Kandt C. dxTuber: detecting protein cavities, tunnels and clefts based on protein and solvent dynamics. *J Mol Graph Mod* 2011;29:895–905.
67. DeLano WL. The PyMol molecular graphics system. San Carlos, CA: DeLano Scientific; 2002.
68. Luecke H, Schobert B, Richter HT, Cartailler JP, Lanyi JK. Structure of bacteriorhodopsin at 1.55 Å resolution. *J Mol Biol* 1999;291:899–911.
69. Spassov VZ, Luecke H, Gerwert K, Bashford D. pK(a) Calculations suggest storage of an excess proton in a hydrogen-bonded water network in bacteriorhodopsin. *J Mol Biol* 2001;312:203–219.
70. Grossfield A, Zuckerman DM. Quantifying uncertainty and sampling quality in biomolecular simulations. *Annu Rep Comput Chem* 2009;5:23–48.
71. Kiselnik VV, Malyuk NG, Toryanik AI, Toryanik VM. Effect of pressure and temperature on self-diffusion of water. *Zhurnal Strukturnoi Khimii* 1973;14:963–967.
72. Syrnikov YP. Calculation of the self-diffusion coefficient of water. *J Struct Chem* 1970;11:698–700.
73. Koronakis V, Sharff A, Koronakis E, Luisi B, Hughes C. Crystal structure of the bacterial membrane protein TolC central to multidrug efflux and protein export. *Nature* 2000;405:914–919.
74. Mikolosko J, Bobyk K, Zgurskaya HI, Ghosh P. Conformational flexibility in the multidrug efflux system protein AcrA. *Structure* 2006;14:577–587.
75. Symmons MF, Bokma E, Koronakis E, Hughes C, Koronakis V. The assembled structure of a complete tripartite bacterial multidrug efflux pump. *Proc Natl Acad Sci USA* 2009;106:7173–7178.
76. Tornroth-Horsefield S, Gourdon P, Horsefield R, Brive L, Yamamoto N, Mori H, Snijder A, Neutze R. Crystal structure of AcrB in complex with a single transmembrane subunit reveals another twist. *Structure* 2007;15:1663–1673.
77. Raetz CR. Enzymology, genetics, and regulation of membrane phospholipid synthesis in *Escherichia coli*. *Microbiol Rev* 1978; 42:614–659.
78. Murakami S. Multidrug efflux transporter, AcrB—the pumping mechanism. *Curr Opin Struct Biol* 2008;18:459–465.
79. Pos KM. Drug transport mechanism of the AcrB efflux pump. *Biochim Biophys Acta* 2009;1794:782–793.
80. Nagle JF, Morowitz HJ. Molecular mechanisms for proton transport in membranes. *Proc Natl Acad Sci USA* 1978;75:298–302.
81. Gutman M, Nachliel E. Time-resolved dynamics of proton transfer in proteinous systems. *Annu Rev Phys Chem* 1997;48:329–356.
82. Zundel G. Proton polarizability and proton transfer processes in hydrogen bonds and cation polarizabilities of other cation bonds: their importance to understand molecular processes in electrochemistry and biology. *Trends Phys Chem* 1992;3:129–156.